Backward runaway electrons in a subnanosecond air discharge at atmospheric pressure

VICTOR F. TARASENKO,[1,2] IGOR' D. KOSTYRYA,[1] AND DMITRY V. BELOPLOTOV[1,2]

[1]Russian Academy of Science, Institute of High Current Electronics, Tomsk 634055, Russia
[2]National Research Tomsk State University, Tomsk 634050, Russia

Abstract

In the paper, we study the conditions for the generation of backward runaway electrons through a grounded grid cathode in atmospheric pressure air at high-voltage pulses with a full width at half maximum of 1 ns and risetime of 0.3 ns applied to the gap from a SLEP-150 pulser. The study confirms that backward runaway electrons and X-rays do arise near grid cathodes in atmospheric pressure air. It is shown that the current of the backward beam and the X-rays from the gas diode depend differently on the interelectrode distance. The average X-ray exposure dose in a pulse is more than 3.5 mR.

Keywords: Atmospheric pressure air; Nanosecond discharge; Runaway electrons beam; X-rays

1. INTRODUCTION

Nanosecond and subnanosecond diffuse discharges in air and other gases at atmospheric pressure in an inhomogeneous electric field have drawn much attention in recent years (see, e.g., Edited Collection by Tarasenko, 2014, and references therein). The diffuse form of discharge in an inhomogeneous electric field at elevated pressures owes to the generation of runaway electrons and X-rays (Tarasova *et al.*, 1974; Tarasenko *et al.*, 2003, 2008*a*; Baksht *et al.*, 2009; Levko *et al.*, 2012). This type of discharge was given the name a runaway electron preionized diffuse discharge or shortly REP DD (Baksht *et al.*, 2009). Research in this type of discharge and in the generation of a supershort avalanche electron beam (SAEB), as proposed elsewhere (Tarasenko *et al.*, 2008*a*, *b*), gave an unexpected result: A backward beam of fast electrons was detected downstream of a grid cathode (Tarasenko *et al.*, 2010).

Time-resolved studies, including those with picosecond resolution, show that the current of backward fast electrons downstream of the cathode depends strongly on the anode material (Baksht *et al.*, 2013; Kostyrya *et al.*, 2013; Tarasenko *et al.*, 2010, 2013). In the same gas diode design, the amplitude of the backward beam current with a tantalum anode is higher than that with an aluminum anode.

Analysis of the available data shows that fast electrons moving backward through a grid cathode were detected for the first time in helium and neon at low pressure and voltage of several kilovolts applied to the gap (Bokhan & Sorokin, 1985*a*, *b*). Two beams of fast electrons were observed in the gap: One beam moved through the grid anode and the other moved backward through the grid cathode. For the gap 0.5 mm, the limiting pressure at which the backward beam was detected was 38 Torr for neon and 90 Torr for helium. The phenomenon was explained by ion injection from the gap through the grid cathode.

At the same time, the generation of a backward runaway electron beam (BRAEB) in atmospheric pressure air was also detected within less than 0.5 ns after applying a voltage pulse of higher amplitude and shorter risetime (Baksht *et al.*, 2013; Kostyrya *et al.*, 2013; Tarasenko *et al.*, 2010, 2013). The so short time left almost no chance for ions to move and more so to be injected into the region downstream of the grid cathode. According to research data, the angle of electron beam generation in atmospheric pressure air under similar conditions was higher than 2π (Tarasenko *et al.*, 2008*a*, *b*). However, the above data were obtained on pulsers with negative polarity, making impossible the arrangement of a collector downstream of the high-voltage cathodes.

The foregoing suggests that BRAEBs can be generated in helium and neon at a pressure of tens of Torr (Bokhan & Sorokin, 1985*a*, *b*) and in air at atmospheric pressure (Baksht *et al.*, 2013; Kostyrya *et al.*, 2013; Tarasenko *et al.*, 2010, 2013). However, the conditions for the generation of a

backward beam in atmospheric pressure air and its parameters are poorly understood and so is the mechanism of the phenomenon.

The present paper studies the conditions under which a BRAEB is generated in air through a grid cathode for which we use different cathode designs and anodes made of Al, Ta, and stainless steel. The backward beam current and X-ray exposure dose are measured with nanosecond and picosecond resolution. The study continues our research reported elsewhere (Baksht *et al.*, 2013; Kostyrya *et al.*, 2013; Tarasenko *et al.*, 2010, 2013). Note that we have not managed to find any other papers which report on the generation of BRAEBs in air and other gases at atmospheric pressure.

2. EXPERIMENTAL SETUP AND MEASURING TECHNIQUE

In our experiments, we used a SLEP-150 pulser capable of producing voltage pulses of negative and positive polarity (Tarasenko *et al.*, 2011; Kostyrya *et al.*, 2012) at negative polarity, a SAEB with $\sim 6 \cdot 10^{10}$ electrons was detected in atmospheric pressure air downstream of an Al foil anode 10-μm-thick (Kostyrya *et al.*, 2012). For the generation of a BRAEB, a voltage pulse of positive polarity with an amplitude of $\cong 150$ kV and full width at half maximum (FWHM) of $\cong 1$ ns was applied to the high-voltage electrode of a gas diode. The voltage risetime was determined by a peaking switch and was $\cong 0.3$ and $\cong 0.4$ ns at negative and positive polarity, respectively. Figure 1a shows a schematic of the gas diode with a collector for operation with voltage pulses of positive polarity.

The anode of the gas diode was 38 mm in diameter and represented a flat disk 3 mm thick with rounded edges. The anode side facing the cathode was made of aluminum, stainless steel or tantalum. The cathode (7) was a grid of parallel steel wires of diameter 0.2 or 0.4 mm stretched with a step of 3, 4, 6 or 8 mm on a flat steel ring 3 mm thick. Additionally, we used grid cathodes made of wire of diameter 0.4 mm with square meshes of size 2×2 and 1×1 mm^2, a tube cathode from foil, and a needle cathode. The steel ring (5) had a hole of diameter 62 mm at its center and was fixed to the flange of the gas diode. On the other side of the ring there was an Al foil of thickness 10 μm reinforced with a grid of transparency 90%. For measuring the electron beam, different collectors were placed downstream of the foil (8) which was also fixed to the flange of the gas diode. The grid-cathode (7) and the foil (8) were spaced by 3 mm, but their separation could be changed to 6, 9, and 12 mm by using additional rings.

The total number of electrons was measured using the collector with a receiving part of diameter 56 mm (9) shown in Figure 1a. For measuring the pulse width of the backward beam with picosecond and subnanosecond resolution, a collimator and a diaphragm were used. For picosecond measurements, we used a collector with a receiving part of diameter 3 mm and a collimator with a thickness of 5 mm and hole

diameter of 1 mm placed downstream of the foil (8). This made it possible to measure beam current pulses with a FWHM of up to 25 ps (Tarasenko *et al.*, 2012). Using a collector with a receiving part diameter of 20 mm and a diaphragm with a hole diameter of 18 mm, the time resolution of the measuring system reached 80 ps (Tarasenko, 2011). The electron beam attenuation was measured using Al foil filters of different thickness, and the X-ray attenuation using Cu foil filters of different thickness. The filters were placed close to the Al foil through which the backward beam was extracted and were connected to the gas diode case along the entire perimeter.

The electron beam moving forward (SAEB) was recorded at negative polarity. The cathode was a grid of parallel steel wires of diameter 0.2 mm stretched with a step of 4 mm on a flat steel ring of diameter 40 mm. The anode was an Al foil 10 μm thick reinforced with a grid of transparency 90%.

For registration electrical signals with picosecond and subnanosecond resolution, we used a LeCroy WaveMaster 830Zi-A digital real-time oscilloscope (up to 30 GHz, 80 GS/s). The collimator with a 1-mm hole allowed measurements of the runaway electron beam parameters without additional signal attenuators. The X-ray exposure dose was measured with Arrow-Tech dosimeters (Model 138). The dose per pulse was estimated from 50 pulses for the Ta anode, from 100 pulses for the stainless steel anode, and from 200 pulses for the Al anode. Imprints of the electron beam and X-rays were recorded on RF (radiographic film)-3 film. Images of the discharge were taken with a Zenit film camera as viewed from the grounded grid and from its side at positive polarity. The Al foil (8) located downstream of the grid (7) was removed.

3. MEASUREMENT RESULTS

In the study, we measured the BRAEB current (I_{BRAEB}) and X-ray with tantalum, stainless steel, and aluminum anodes and cathodes of different designs. Moreover, the range and number of measured parameters was greatly extended as compared to our previous studies (Baksht *et al.*, 2013; Kostyrya *et al.*, 2013; Tarasenko *et al.*, 2010, 2013). The BRAEB and X-rays were measured at positive polarity, and the SAEB at negative polarity of the SLEP-150 pulser. Before measurements, each fresh electrode was conditioned by several tens of pulses.

Figure 2 shows waveforms of the voltage from the capacitive voltage divider shown in Figure 1 and waveforms of the backward beam for the Ta and Al anodes at picosecond and subnanosecond resolution.

The waveforms of the voltage allow for a 60 ps delay of arrival of the reflected voltage wave at the capacitive voltge divider. The shape and amplitude of voltage pulses varied little with the anode material. The average voltage amplitude in 50 pulses for the Al anode is a mere 10% higher than that for the Ta anode. Note that the amplitude and risetime of the voltage from the capacitive divider at positive polarity were
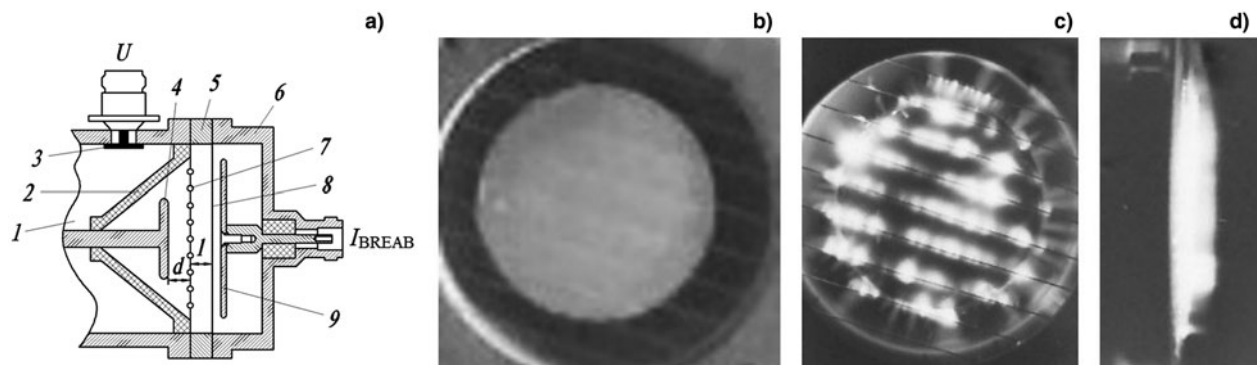
Fig. 1. Gas diode and measuring system (a): 1 – coaxial line, 2 – insulator, 3 – capacitive voltage divider, 4 – anode, 5 – steel ring, 6 – collector box, 7 – wire grid, 8 – foil, and 9 – collector receiving part of diameter 56 mm. Images of the gas diode in a pulse without the collector, metal ring, and foil: View from the grid cathode (b, c) and side view (d) with no discharge plasma (b) and with (c, d); the anode diameter is 38 mm, the wire separation is 4 mm.

higher than those at negative polarity (SAEB generation), while all other things being equal. This agrees with data on the effect of polarity inversion (Shao *et al.*, 2014).

At picosecond resolution (Fig. 2b), the BRAEB was measured by the collector with a receiving part diameter of 3 mm through the 1 mm collimator hole. Like in our previous studies (Tarasenko *et al.*, 2010, 2013; Baksht *et al.*, 2013; Kostyrya *et al.*, 2013), the amplitude of the backward beam for the Ta anode was much higher than that for the Al anode at the same voltage amplitudes. However, the FWHM of
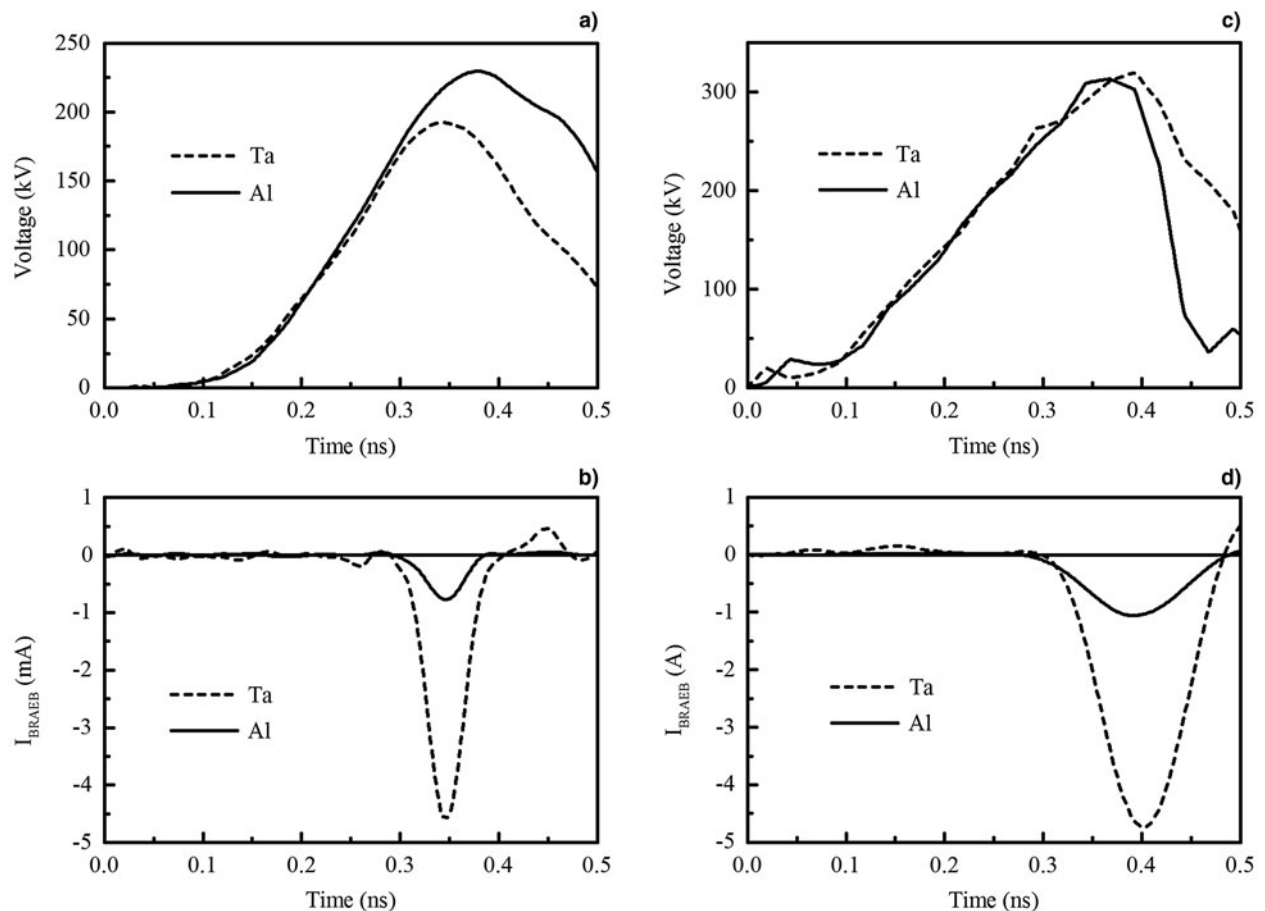

Fig. 2. Waveforms of the voltage from the capacitive voltage divider (a, c) and backward beam current at picosecond (b), and subnanosecond (d) resolution for the Ta and Al anodes, grid cathode composed of wires of diameter 0.2 mm spaced by 4 mm, and interelectrode gap 4 mm.

the backward beam with maximum current amplitudes in both cases was about the same, measuring 40–45 ps. Note that the collimator and collector with a receiving part diameter of 3 mm allow one to measure only a small part of the backward beam, and this decreases the current pulse width compared with that from the entire foil surface both for backward beams and for SAEBs (Tarasenko *et al.*, 2004, 2008*a*, 2013).

At subnanosecond resolution (Fig. 2d), the backward beam was measured by the collector with a receiving part diameter of 20 mm through the 18 mm diaphragm hole The FWHM of the backward beam for the Ta and Al anodes was $\cong 95$ and $\cong 115$ ps, respectively. The FWHM of the backward beam measured by the collector with a receiving part diameter of 20 mm differed little from the FWHM over the entire surface of the foil (8) in Figure 1, but the number of backward runaway electrons was about two times smaller than their number from the entire foil surface.

For increasing the backward beam amplitude, the cathode design and the wire separation were optimized (Fig. 3).

The highest backward beam amplitude was obtained for the cathode consisting of parallel wires of diameter 0.2 mm spaced by 4 mm. Increasing the wire diameter increased their optimum separation.

The amplitude of the backward beam depended on the number of parallel wires. Figure 4 shows the beam current amplitude against the number of cathode wires.

The first wire was arranged at the center and its length was equal to the diameter of the ring (5) in Figure 1. The next two wires were arranged symmetrically on both sides of the first wire and so were the next two. It is seen from Figure 4 that increasing the number of wires to 5, greatly increased the backward beam amplitude, and further increasing their number caused saturation of the beam amplitude.

The use of the grid cathode with square meshes and smaller wire separation decreased the backward beam amplitude. For the cathode with a mesh size of 2×2 mm^2 and wire

thickness of 0.4 mm, the number of backward runaway electrons decreased almost ten times. Imprints on the RF-3 film exposed to the backward beam and X-rays for the mesh grid cathode are shown in Figures 5a and 5b.

For all four imprints, the separation between the cathode (7) and foil (8) was $l = 3$ mm (Fig. 1). The RF-3 film in a black paper envelope of thickness 120 μm was placed downstream of the foil. All imprints reveal a clearly defined grid structure. With the cathode comprising only a grid, several pulses were sufficient for noticeable blackening of the film. At the same number of pulses, the highest degree of blackening was observed when the backward beam amplitude was highest. With the cathode comprising wires of diameter 0.2 mm spaced from each other and from the Ta anode by 4 mm, the blackening of the film was maximal. A single pulse was sufficient for total film exposure. The number of backward runaway electrons, in this case, was $\sim 7 \cdot 10^9$.

The imprint shown in Figure 5c was obtained with a cathode representing a ring of diameter 20 mm, height 4 mm, and wall thickness 100 μm placed on a grid with a mesh size of 2×2 mm^2 facing the anode. With this cathode at a ring–anode separation of 4 mm, the amplitude of the backward beam decreased 3.7 times compared with that in Figures 5a and 5b. At the center of the imprint, one can see severe ring-shaped blackening of the film.

The imprint in Figure 5d was obtained with a cathode representing a sewing needle of height 4 mm. With this cathode, the amplitude of the backward runaway beam decreased greatly such that the beam was hardly detectable against the background of electromagnetic noise. In this case, to obtain a clear imprint, the exposure was increased to 200 pulses. At the center of the imprint, one can see a bright spot which shows the position of the needle cathode. It can be supposed that the main film exposure for the ring and needle cathodes owes mostly to bremsstrahlung X-rays from the anode. Earlier studies also revealed a decrease in SAEB amplitude for a needle cathode compared with tubular
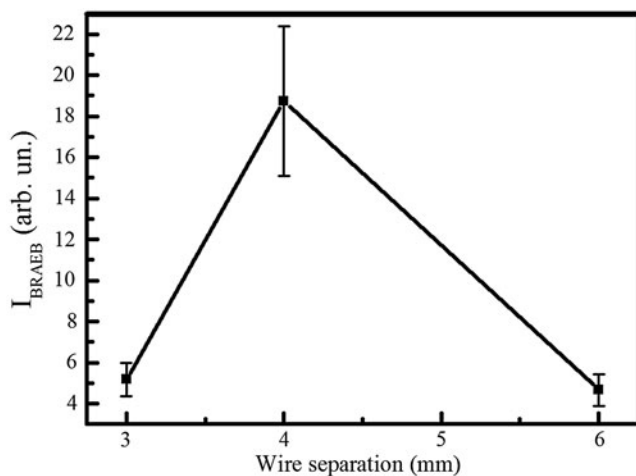

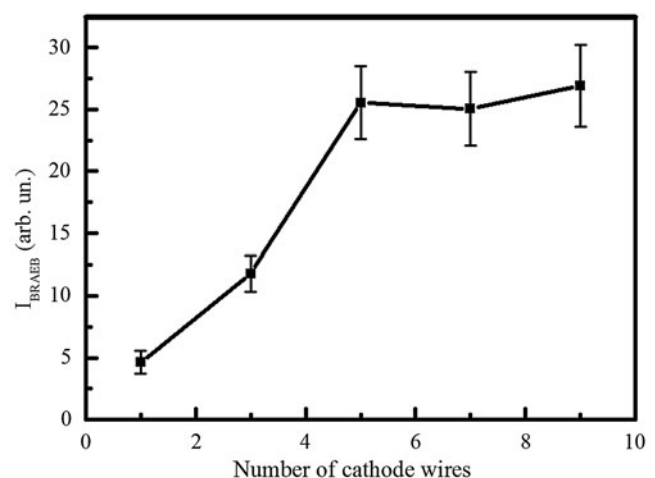**Fig. 3.** Backward beam amplitude versus the wire separation for wires of diameter 0.2 mm.

Fig. 4. Backward beam current versus the number of cathode wires of diameter 0.2 mm.
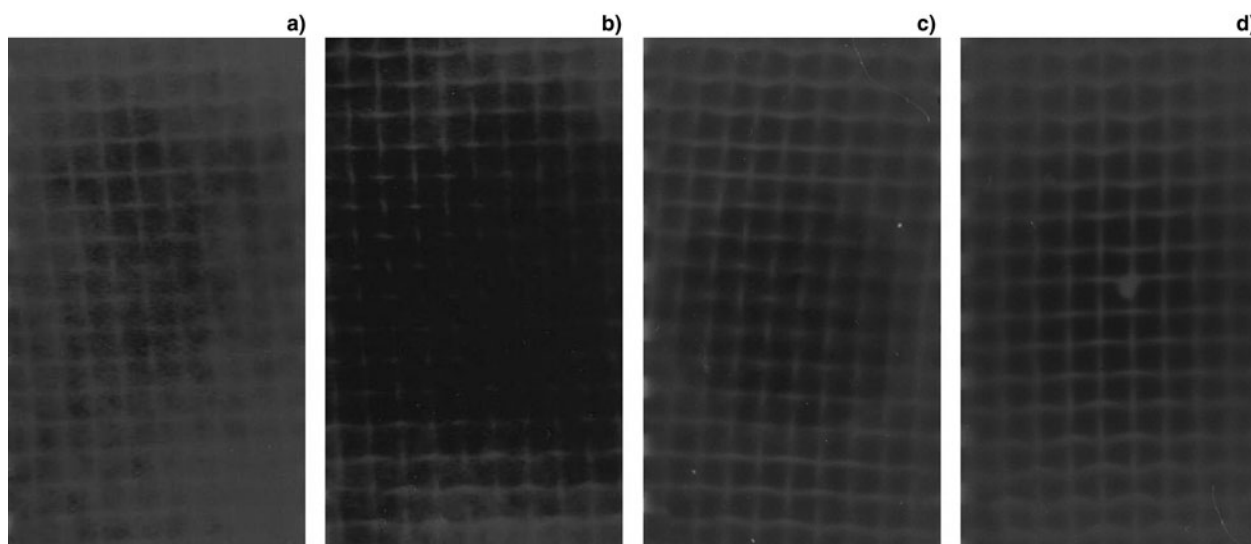
Fig. 5. RF-3 film exposed to the backward beam and X-rays within 5, 10, 50, and 200 pulses for different cathode designs: Grid with a mesh size of 2×2 mm^2 (a, b); foil ring of diameter 20 mm, height 4 mm, and thickness 100 μm on a grid with a mesh size of 2×2 mm^2 (c); needle of height 4 mm on a grid with a mesh size of 2×2 mm^2 (d). The interelectrode distance is 5 (a, b) and 4 mm (c, d).

and spherical cathodes (Tarasenko *et al.*, 2004). Increasing the number of runaway electrons requires a longer sharp edge of the cathode with a small curvature radius (Tarasenko, 2011; Kostyrya *et al.*, 2012) without any mutual shielding from adjacent wires.

With the grid in which the mesh size was 1×1 mm^2, no backward electron beam was detected. The same was observed when the foil (8) was brought close to the grid (7). This can be explained by a decrease in electric field strength near the close-spaced grid wires as the grid–foil separation is decreased.

At increasing distance between cathode (wire grid) and collector through both increasing distance between cathode (7) and foil (8) or moving of the collector away from the foil (8)
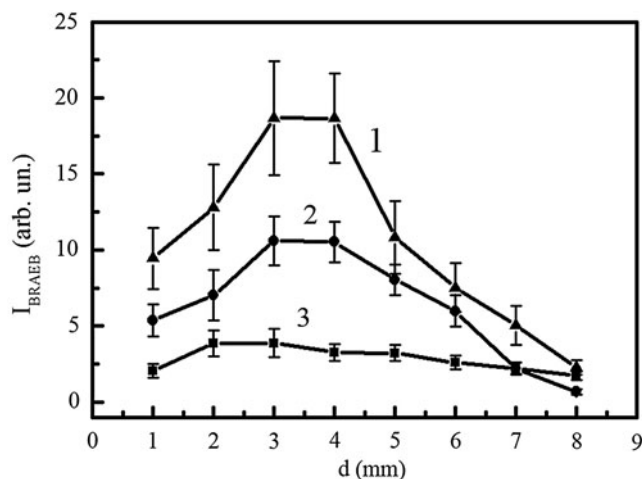

Fig. 6. Number of backward electrons versus the interelectrode distance in a discharge in atmospheric pressure air with the cathode consisting of wires of diameter 0.2 mm spaced by 4 mm for the anodes made of tantalum – 1, stainless steel – 2, and aluminum – 3.

with keeping of distance between cathode (7) and foil (8) at 3 mm, the number of backward runaway electrons decreased.

Figure 6 shows dependencies of the number of backward electrons on the interelectrode distance in a discharge in atmospheric pressure air.

The dependencies were obtained using the collector with a receiving part diameter of 56 mm. The use of the collector distorted the pulse shape of the beam current but allowed us to determine the number of electrons downstream of the entire foil surface. For all anode materials, there exists an optimum interelectrode distance at which the highest number of runaway electrons is detected downstream of the cathode. The number of backward electrons for the stainless steel anode is higher than that for the Al anode but lower than their number for the Ta anode. This fits the ratio of atomic numbers for these materials. The largest number of backward electrons was detected for the Ta anode and was $\sim 7 \cdot 10^9$, which agrees with data of our previous studies (Baksht *et al.*, 2013; Kostyrya *et al.*, 2013; Tarasenko *et al.*, 2013). The number of backward electrons under optimum conditions was an order of magnitude lower than that of SAEB electrons with optimum cathode and gas diode designs at negative polarity; the number of SAEB electrons downstream of the anode was $6.2 \cdot 10^{10}$ in a pulse (Kostyrya *et al.*, 2012). The maximum in the energy distribution of the backward runaway beam was lower than that in the SAEB distribution, as was the case in our previous studies (Baksht *et al.*, 2013; Kostyrya *et al.*, 2013; Tarasenko *et al.*, 2013). The maximum energy of the backward beam was lower than the maximum SAEB energy. The electron energy in gas diodes at voltage pulses of negative polarity was studied in detail elsewhere (Tarasenko *et al.*, 2005, 2008*a*, *b*, 2011; Mesyats *et al.*, 2011; Alekseev *et al.*, 2012; Zhang *et al.*, 2014; Kozyrev *et al.*, 2015).

Figure 7 shows dependencies of the X-ray exposure dose on the interelectrode distance in a discharge in atmospheric pressure for different anode materials.

As expected, the maximum exposure doses were obtained for the Ta anode. However, the maximum doses were produced with smaller interelectrode distances than those at which the number of backward electrons was maximal. This result differs from data on the interelectrode distance dependence of SAEB and X-rays produced at negative polarity of the SLEP-150 pulser (Alekseev *et al.*, 2012). When the SLEP-150 pulser operates at negative polarity, the X-rays are produced due to electron bombardment of a foil anode made of metal with a high atomic number and are extracted through the same foil anode. This causes substantial attenuation of low-energy X-ray quanta. When the SLEP-150 pulser operates at positive polarity, the X-rays are also produced on deceleration of fast electrons at a metal anode with a high atomic number but their extraction from the gas diode is through a thin Al foil. This reduces the absorption of soft X-rays. The decrease in X-ray absorption together with an increase in gap voltage at positive polarity made it possible to increase the X-ray dose in a pulse several times (to 3.5 mR).

4. DISCUSSION

The reported research results confirm the possibility of generation of a BRAEB and the main trends of this interesting phenomenon detected in atmospheric pressure air (Baksht *et al.*, 2013; Kostyrya *et al.*, 2013; Tarasenko *et al.*, 2010, 2013). By optimizing the cathode design and interelectrode gap we have managed to increase the X-ray dose at positive polarity to 3.5 mR. It is found that the generation of backward beams with highest amplitudes requires cathodes composed of wires spaced by ≥4 mm.
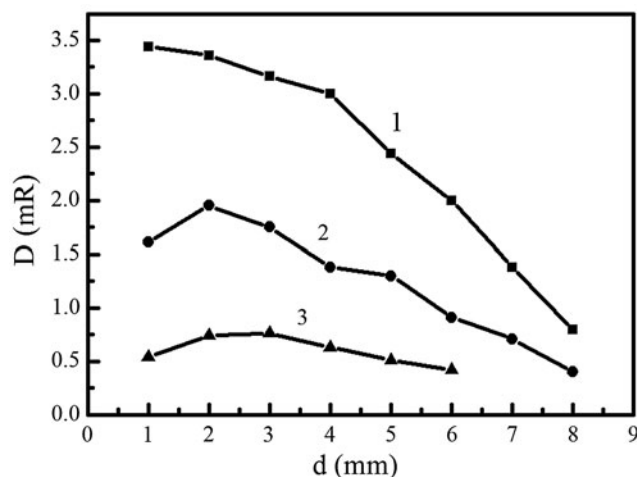
The main question to be answered is the cause of appearance of runaway electrons downstream of the cathode. Reasoning from the fact that the electric field penetrates into this cathode region (Baksht *et al.*, 2013; Kostyrya *et al.*, 2013; Tarasenko *et al.*, 2013), let us elucidate whether its value is high enough for electron runaway. For this purpose, we calculated the distribution of the electric field strength in the gap along the line near its symmetry axis. The simulation was performed using an ELCUT 5.1 Professional program (http://elcut.ru/allnews/elcut51_r.htm). The calculation results are presented in Figure 8.

From the calculations it follows that the maximum electric field strength is observed on the region near the wire surface and its value under these conditions is higher than 1 MV cm^{-1}. The so high electric field explains the appearance of first electrons at the cathode, including the wire side opposite the anode (between the grid and the foil) and the transition of part of the electrons to the runaway mode. However, this is insufficient for the number of backward electrons to be large. The high electric field between the grid and foil provides the generation of first runaway electrons. The generation of a considerable number of electrons ($\sim 7{\cdot}10^9$ for the Ta anode) requires an ionization wave front moving from the wire cathode backward to its downstream region as well as toward the anode.

Figure 1 shows images of the gas diode without the collector, metal ring, and foil as viewed from the grid cathode (Figs. 1b and 1c) and from its side (Fig. 1d) with no discharge plasma (Fig. 1b) and with the plasma in a pulse at positive polarity (Figs. 1c and 1d). It is seen that the dense plasma glows at the cathode wires (Fig. 1c) and that the radiation is detected downstream of the cathode at a distance of about 10 mm from the ring to which the cathode wires are attached (Fig. 1d). These images confirm the backward ionization wave propagation. Most of the runaway electrons are
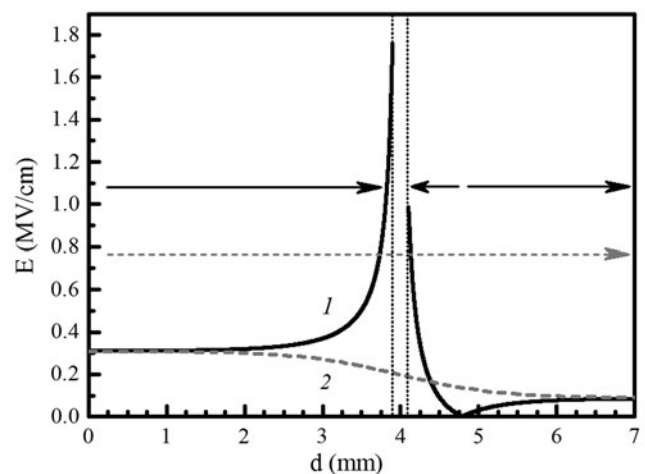

Fig. 7. X-ray exposure dose produced by the backward beam versus the interelectrode distance for the Ta anode – 1, stainless steel anode – 2, and Al anode – 3. The cathode consists of wires of diameter 0.2 mm spaced by 4 mm.

Fig. 8. Electric field strength distribution between the anode (at the left) and grounded foil (at the right) along the line passing through the wire – 1 and between the wires – 2 near the gap symmetry axis. The wire boundaries are marked by vertical dotted lines; the direction of the field vector is indicated by arrows. The interelectrode distance and the wire separation is 4 mm.

generated at the ionization wave front (Tarasenko *et al.*, 2003, 2008*a*, *b*, 2010; Baksht *et al.*, 2009; Tarasenko, 2011; Kostyrya *et al.*, 2012; Shao *et al.*, 2012, 2013; Zhang *et al.*, 2013, 2014).

Surely, the radiation from the dense plasma is more intense mostly in the gap between the grid cathode and plane anode. Hence, the number of runaway electrons in the gap is much larger and their energy is higher than that of backward electrons. When the potential electrode is the anode, it is very difficult to detect a SAEB. The generation of a SAEB with a large number of runaway electrons can be judged from intense (up to 3.5 mR) X-rays from the anode. However, when the pulser polarity is reversed with replacement of the plane potential anode by the grid cathode and also the mesh cathode by the Al foil of thickness 10 μm, which becomes the anode, stable SAEB generation is observed. The SAEB amplitude in atmospheric pressure air reaches 100 A at a FWHM of ∼100 ps which corresponds to $6.2 \cdot 10^{10}$ fast electrons in a pulse (Kostyrya *et al.*, 2012).

As it follows from Figures 6 and 7, the number of backward runaway electrons and X-ray exposure doses depend largely on the anode material. The use of a metal anode with a large atomic number increases the number of backward electrons and the X-ray exposure dose. The increase in the exposure dose owes to an increase in bremsstrahlung X-ray intensity generated by runaway electrons accelerated between the grid cathode and anode with a large atomic number. We suppose that the increase in the number of backward runaway electrons, in this case, is due to participation of bremsstrahlung X-rays from the anode in the formation of an ionization wave whose front moves backward and to additional electron emission from the cathode wires. Apparently, the X-rays from the anode are significant in early stage of the formation of dense plasma at the cathode when the number of backward runaway electrons is small. According to the data of our studies, it can be stated that most of the runaway electrons at a subnanosecond voltage pulse risetime is generated due to electric field strength amplification near the polarized ionization wave front (Tarasenko *et al.*, 2003, 2008*a*, *b*, 2010, Baksht *et al.*, 2009; Tarasenko, 2011; Kostyrya *et al.*, 2012; Shao *et al.*, 2012, 2013; Zhang *et al.*, 2013, 2014).

5. CONCLUSION

The results reported in the paper confirm the possibility of generation of a backward runaway electron beam. It is found that the highest amplitudes of the backward beam are attained using a plane anode made of metal with a high atomic number, in our experiments, tantalum. It is shown that the optimum interelectrode distance for the generation of backward beams are larger than those for the generation of maximum exposure doses. The generation of backward runaway electrons owes to electric field penetration through the widely spaced grid and backward propagation of the dense plasma due to electric field amplification near the grid cathode with a small curvature radius. It is supposed

that preionization of the region ahead of the backward dense plasma front by bremsstrahlung X-rays from the anode influences the amplitude of the backward beam.

REFERENCES

ALEKSEEV, S.B., BAKSHT, E.KH., BOICHENKO, A.M., KOSTYRYA, I.D., TARASENKO, V.F. & TKACHEV, A.N. (2012). X-ray radiation and runaway electron beam spectra at a nanosecond discharge in atmospheric-pressure air. *Tech. Phys.* **57**, 1192–1198.

BAKSHT, E.KH., BURACHENKO, A.G., KOSTYRYA, I.D., LOMAEV, M.I., RYBKA, D.V., SHULEPOV, M.A. & TARASENKO, V.F. (2009). Runaway-electron-preionized diffuse discharge at atmospheric pressure and its application. *J. Phys. D: Appl. Phys.* **42**, 185201.

BAKSHT, E.KH., KOZYREV, A.V., KOSTYRYA, I.D., RYBKA, D.V. & TARASENKO, V.F. (2013). Fast electrons behind the plane-grid cathode at nanosecond discharge in atmospheric pressure air. *High Volt. Eng.* **39**, 2138–2144.

BOKHAN, P.A. & SOROKIN, A.P. (1985*a*). Open discharge and electron beam generation: Mechanisms, properties, and use for laser pumping of average pressure). *J. Tech. Phys.* **55**, 88–95. (in Russian).

BOKHAN, P.A. & SOROKIN, A.P. (1985*b*). Electron beam formation in an overcharged layer in a gas discharge at average pressure. *J. Tech. Phys.* **55**, 1168–1170. (in Russian).

KOSTYRYA, I.D., RYBKA, D.V. & TARASENKO, V.F. (2012). The amplitude and current pulse duration of a supershort avalanche electron beam in air at atmospheric pressure. *Instrum. Exp. Tech.* **55**, 72–77.

KOSTYRYA, I.D., RYBKA, D.V., TARASENKO, V.F., KOZYREV, A.V. & BAKSHT, E.KH. (2013). Occurrence of runway electrons behind the cathode under subnanosecond breakdown of air at atmospheric pressure. *Rus. Phys. J.* **55**, 1493–1496.

KOZYREV, A.V., KOZHEVNIKOV, V.YU., VOROBYEV, M.S., BAKSHT, E.KH., BURACHENKO, A.G., KOVAL, N.N. & TARASENKO, V.F. (2015). Reconstruction of electron beam energy spectra for vacuum and gas diodes. *Laser Part. Beams* **33**, 183–192.

LEVKO, D., KRASIK, YA.E. & TARASENKO, V.F. (2012). Present status of runaway electron generation in pressurized gases during nanosecond discharges. *Int. Rev. Phys.* (*IREPHY*) **6**, 165–195.

MESYATS, G.A., REUTOVA, A.G., SHARYPOV, K.A., SHPAK, V.G., SHUNAILOV, S.A. & YALANDIN, M.I. (2011). On the observed energy of runaway electron beams in air. *Laser Part. Beams* **29**, 425–435.

SHAO, T., TARASENKO, V.F., ZHANG, CH., BAKSHT, E.KH., YAN, P. & SHUT'KO, YUV. (2012). Repetitive nanosecond-pulse discharge in a highly nonuniform electric field in atmospheric air: X-ray emission and runaway electron generation. *Laser Part. Beams* **30**, 369–378.

SHAO, T., TARASENKO, V.F., ZHANG, CH., BELOPLOTOV, D.V., YANG, W., LOMAEV, M.I., ZHOU, ZH., SOROKIN, D.A. & YAN, P. (2014). Abnormal polarity effect in nanosecond-pulse breakdown of SF6 and nitrogen. *Phys. Lett. A* **378**, 1828–1833.

SHAO, T., TARASENKO, V.F., ZHANG, CH., BURACHENKO, A.G., RYBKA, D.V., KOSTYRYA, I.D., LOMAEV, M.I., BAKSHT, E.KH. & YAN, P.

(2013). Application of dynamic displacement current for diagnostics of subnanosecond breakdowns in an inhomogeneous electric field. *Rev. Sci. Instrum.* **84**, 053506.

TARASENKO, V.F. (2011). Parameters of a supershort avalanche electron beam generated in atmospheric-pressure air. *Plasma Phys. Rep.* **37**, 409–421.

Tarasenko, V.F. (Ed.). (2014). *Runaway Electron Preionized Diffuse Discharges*. New York, USA, Published by Nova Science Publishers, Inc.

TARASENKO, V.F., BAKSHT, E.KH., BURACHENKO, A.G., KOSTYRYA, I.D., LOMAEV, M.I. & RYBKA, D.V. (2008*a*). Generation of supershort avalanche electron beams and formation of diffuse discharges in different gases at high pressure. *Plasma Dev. Oper.* **16**, 267–298.

TARASENKO, V.F., BAKSHT, E.KH., BURACHENKO, A.G., KOSTYRYA, I.D., LOMAEV, M.I. & RYBKA, D.V. (2008*b*). Supershort avalanche electron beam generation in gases. *Laser Part. Beams* **26**, 605–617.

TARASENKO, V.F., BAKSHT, E.KH., BURACHENKO, A.G., KOSTYRYA, I.D., LOMAEV, M.I. & RYBKA, D.V. (2010). Supershort avalanche electron beams and x-rays in atmospheric-pressure air. *IEEE Trans. Plasma Sci.* **38**, 741–750.

TARASENKO, V.F., BAKSHT, E.KH., EROFEEV, M.V., KOSTYRYA, I.D., RYBKA, D.V. & SHUTKO, Y.V. (2013). New features of the generation of runaway electrons in nanosecond discharges in different gases. *IEEE Trans. Plasma Sci.* **41**, 2931–2940.

TARASENKO, V.F., KOSTYRYA, I.D., BAKSHT, E.KH. & RYBKA, D.V. (2011). SLEP-150M compact supershort avalanche electron beam accelerator. *IEEE Trans. Dielectr. Electr. Insul.* **18**, 1250–1255.

TARASENKO, V.F., ORLOVSKII, V.M. & SHUNAILOV, S.A. (2003). Forming of an electron beam and a volume discharge in air at atmospheric pressure. *Rus. Phys. J.* **46**, 325–327.

TARASENKO, V.F., RYBKA, D.V., BURACHENKO, A.G., LOMAEV, M.I. & BALZOVSKY, E.V. (2012). Measurement of extreme-short current pulse duration of runaway electron beam in atmospheric pressure air. *Rev. Sci. Instrum.* **83**, 086106.

TARASENKO, V.F., SKAKUN, V.S., KOSTYRYA, I.D., ALEKSEEV, S.B. & ORLOVSKII, V.M. (2004). On formation of subnanosecond electron beams in air under atmospheric pressure. *Laser Part. Beams* **22**, 75–82.

TARASENKO, V.F., SHPAK, V.G., SHUNAILOV, S.A. & KOSTYRYA, I.D. (2005). Supershort electron beam from air filled diode at atmospheric pressure. *Laser Part. Beams* **23**, 545–551.

TARASOVA, L.V., KHUDYAKOVA, L.N., LOIKO, T.V. & TSUKERMAN, V.A. (1974). The fast electrons and X-Ray radiation of nanosecond pulsed discharges in gases under 0.1-760 Torr. *J. Tech. Phys.* **44**, 564–568.

ZHANG, CH., TARASENKO, V.F., SHAO, T., BAKSHT, E.KH., BURACHENKO, A.G., YAN, P. & KOSTYRAY, I.D. (2013). Effect of cathode materials on the generation of runaway electron beams and X-rays in atmospheric pressure air. *Laser Part. Beams* **31**, 353–364.

ZHANG, CH., TARASENKO, V.F., SHAO, T., BELOPLOTOV, D.V., LOMAEV, M.I., SOROKIN, D.A. & YAN, P. (2014). Generation of supershort avalanche electron beams in SF$_6$. *Laser Part. Beams* **32**, 331–341.